Non-Markovian effects on the two-dimensional magnetotransport: Low-field anomaly in magnetoresistance

Vadim V. Cheianov,[1] A. P. Dmitriev,[2] and V. Yu. Kachorovskii[2]
[1]*NORDITA, Blegdamsvej 17, Copenhagen DK 2100, Denmark*
[2]*A. F. Ioffe Physical-Technical Institute, 26 Polytechnicheskaya Str., Saint Petersburg 194021, Russia*
(Received 16 May 2004; published 8 December 2004)

We discuss classical magnetotransport in a two-dimensional system with strong scatterers. Even in the limit of very low field, when $\omega_c\tau \ll 1$ (ω_c is the cyclotron frequency, τ is the scattering time) such a system demonstrates strong negative magnetoresistance caused by non-Markovian memory effects. A regular method for the calculation of non-Markovian corrections to the Drude conductivity is presented. A quantitative theory of the recently discovered anomalous low-field magnetoresistance is developed for the system of two-dimensional electrons scattered by hard disks of radius a, randomly distributed with concentration n. For small magnetic fields the magentoresistance is found to be parabolic and inversely proportional to the gas parameter, $\delta\rho_{xx}/\rho \sim -(\omega_c\tau)^2/na^2$. In some interval of magnetic fields the magnetoresistance is shown to be linear $\delta\rho_{xx}/\rho \sim -\omega_c\tau$ in a good agreement with the experiment and numerical simulations. Magnetoresistance saturates for $\omega_c\tau \gg na^2$, when the anomalous memory effects are totally destroyed by the magnetic field. We also discuss magnetotransport at very low fields and show that at such fields magnetoresistance is determined by the trajectories having a long Lyapunov region.

DOI: 10.1103/PhysRevB.70.245307 PACS number(s): 73.43.Qt, 05.60.Cd, 05.60.Gg, 73.50.Jt

I. INTORDUCTION

The problem of magnetoresistance in metal and semiconductor structures has been intensively discussed in literature during the past three decades. A large number of both theoretical and experimental papers on this subject was published. Most of these works were devoted to the case of the degenerate two-dimensional electron gas where the electrons move in the plane perpendicular to the magnetic field and scatter on a random impurity potential. In this situation only the electrons with energy close to the Fermi energy participate in conductance and the usual approach based on the Boltzmann equation leads to vanishing magnetoresistance. In other words, the longitudinal resistance ρ_{xx} of the sample does not depend on the magnetic field B. This implies that the explanation of the experimentally observed B dependence of the longitudinal resistance should be sought beyond the Boltzmann theory.

The intense exploration of this area began from the work of Altshuler *et al.*[1] where the experimentally observed in two-dimensional (2D) metals and semiconductor structures negative magnetoresistance (MR), i.e., decreasing ρ_{xx} with increasing B, was explained by quantum interference effects. It was shown that the magnetic field destroys the negative weak localization correction to the conductivity, thus resulting in decreasing longitudinal resistance. Since the first publication on the subject[1] a vast amount of work has been devoted to its further exploration (see for review Ref. 2).

Two years prior to Ref. 1 there appeared a publication[3] where a classical mechanism of negative magnetoresistance was discussed. The mechanism was investigated on the example of a gas of noninteracting electrons scattering on hard disks (antidots). It was shown that with increasing magnetic field there is an increasing number of closed electron orbits which avoid scatterers and therefore are not diffusive (see also recent discussions[4–7] of this mechanism). Electrons occupying these orbits do not participate in diffusion. As a result, the longitudinal resistance turns out to be proportional to the factor $1-P$, where $P=\exp(-2\pi/\omega_c\tau)$ is the probability of the existance of the circular closed orbit, which avoids scatterers (here ω_c is the cyclotron frequency, τ is the scattering time). Another classical mechanism was presented in Ref. 8, where the MR due to non-Markovian dynamics of electrons trapped in some region of space was discussed.

Notwithstanding these developments, the role of classical effects in magnetotransport was underappreciated for a long time. A new boost to the research in this direction was given by Ref. 9, where it was shown that if electrons move in a smooth disorder potential and in a sufficiently strong magnetic fields a phenomenon called "classical localization" occurs. This phenomenon leads to the exponential suppression of the longitudinal resistance: most electrons are trapped in localized equipotential trajectories and do not participate in diffusion. This work was followed by a series of works,[10–17] discussing different aspects of classical magnetotransport in 2D systems. It was shown[11] that for lower magnetic fields near the onset of the classical localization the magnetoresistance is positive, i.e., the longitudinal resistance grows with increasing magnetic field. In Refs. 12 and 13 the combination of smooth disorder and strong scatterers (antidots) was considered. It was shown that in this system under certain conditions there are several regimes of the behavior of magnetoresistance depending on the strength of the magnetic field: first the longitudinal resistance decreases with growing field, then it saturates and then begins to grow.

In Refs. 3–14 magnetoresistance was studied in a situation where the magnetic field is classically strong, that is where the parameter $\beta=\omega_c\tau$ is large. Recently, the region of classically small magnetic fields $\beta \ll 1$ was investigated numerically[15,16] for the case of electrons scattering on strong

scatterers. It was shown[15] that memory effects due to double scattering of an electron on the same disk lead to a negative parabolic magnetoresistance (in Ref. 3, where these processes were not taken into account, exponentially small MR was predicted). The numerical simulations[16] discovered a low-field classical anomaly of the MR. The anomaly was attributed to the memory effects specific for backscattering events. The simulations were performed for the 2D Lorenz gas which is a system of 2D electrons scattering on hard disks randomly distributed in plane with average concentration n. Magnetotransport in this system is characterized by two dimensionless parameters: $\beta=\omega_c\tau$, and the gas parameter $\beta_0=a/l=2na^2$. Here a is the disk radius, ω_c is the cyclotron frequency, $\tau=l/v_F$ is the mean free time and $l=1/2na$ is the mean free path. The anomaly was observed in the case $\beta\ll 1$, $\beta_0\ll 1$. Both the numerical simulations and the qualitative considerations[16] indicated that at zero temperature the MR can be expressed in terms of a dimensionless function $f(z)$ via

$$\frac{\delta\rho_{xx}}{\rho}=-\beta_0 f\left(\frac{\beta}{\beta_0}\right), \tag{1}$$

where ρ is the resistivity for $B=0$. Numerical results[16] suggest that $f(z)\sim z$ as $z\to 0$, yielding

$$\frac{\delta\rho_{xx}}{\rho}\sim -|\omega_c|\tau. \tag{2}$$

The latter expression is in very good agreement with experimental measurements of negative linear MR in random antidot arrays.[18] It is anomalous in two senses. First, it has a non-analytic dependence on the magnetic field. Second, it does not vanish in the limit of vanishing β_0, which is normally regarded as the expansion parameter for the corrections to the Drude-Boltzmann picture. This intriguing behavior calls for a rigorous analytical theory of the effect, which would establish Eq. (1) and enable one to derive the analytical expression for function f.

In this paper we present a detailed theory of the anomaly and give an expression for $f(z)$ (the brief description of our results was given in Ref. 17). We find that at some interval, $0.05\lesssim z\lesssim 2$, function $f(z)$ is linear in agreement with numerical simulations and experiment, but at $z\to 0$ crosses over to a quadratic dependence. Thus, for $\beta\to 0$, Eq. (1) yields $\delta\rho_{xx}/\rho\sim-\beta^2/\beta_0$. The limit $\beta_0\to 0$ should be taken with care. While the small β expansion seems to be singular as a function of β_0, the region of β where this expansion is valid shrinks as $\beta_0\to 0$. For $z\to\infty$, f saturates at some constant value. Therefore, the full variation of $\delta\rho_{xx}/\rho$ is of the order β_0. In other words, the anomalous MR is strong but it exists in a small region of magnetic fields.

II. QUALITATIVE DISCUSSION OF THE PROBLEM

The mechanism proposed in Ref. 6 is linked to the memory effects arising in backscattering events. It has a close relation to the well known nonanalyticity of the virial expansion of transport coefficients,[19–23] which we briefly recall. For $B=0$ the leading nonanalytic correction to resistivity, $\delta\rho$, is due to the processes of return to a scatterer after a single collision on another scatterer [see Fig. 1(a)]. The relative correction, $\delta\rho/\rho$, is proportional to the corresponding backscattering probability, given by the product of $e^{-R/l}\,d\Phi\,dR/l$ (which is the probability to reach scatterer 2 without collision and scatter in the angle $d\Phi$) and the probability p to return without collisions from 2 to 1 (here l is the mean free pass). Assuming $p=\exp(-R/l)$ and integrating over intervals $0<\Phi<a/R$, $a<R<\infty$, one obtains[19–23]

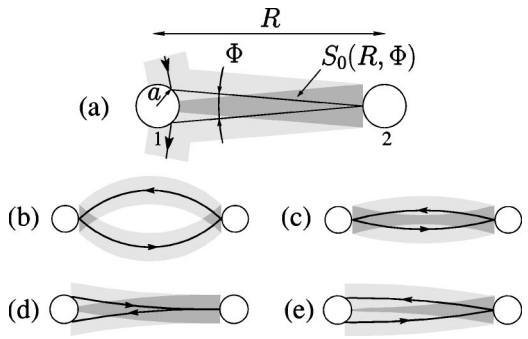

FIG. 1. Backscattering process responsible for leading nonanalytic contribution to the resistivity at $B=0$ (a). For $B\neq 0$, the overlap area, S_B, between two corridors is small at large B (b). For $\Phi=0$, S_B decreases with B (c). For $\Phi\neq 0$ and small B the values of S_B-S_0 for time reversed trajectories have opposite signs (d) and (e).

$$\delta\rho/\rho\sim\int_a^\infty\frac{dR}{l}\int_0^{a/R}d\Phi\,e^{-2R/l}\sim\beta_0\ln(1/2\beta_0). \tag{3}$$

In Ref. 16 it was shown that the probability p is actually larger than $\exp(-R/l)$. Indeed, the exponent $\exp(-R/l)$ can be written as $\exp(-nS)$, where $S=2aR$. It represents the probability of the existence of an empty corridor (free of the centers of the disk) of width $2a$ around the electron trajectory from 2 to 1. However, the passage of a particle from 1 to 2 ensures the absence of the disks centers in the region of width $2a$ around this part of trajectory (from 1 to 2). This reduces the scattering probability on the way back. The correct value of p can be estimated as

$$p(R,\Phi)=\exp(-n(S-S_0))=\exp(-R/l+nS_0(R,\Phi)), \tag{4}$$

where

$$S_0(R,\Phi)=2aR-R^2|\Phi|/2 \tag{5}$$

is the area of the overlap of the two corridors [see Fig. 1(a)]. For example, for $\Phi=0$, we have $S_0=2aR$ and $p=1$, which reflects the obvious fact that the particle cannot scatter, if it travels back along the same path. Taking into account the effect of "empty corridor," we get

$$\frac{\delta\rho}{\rho}\sim\int_a^\infty\frac{dR}{l}\int_0^{a/R}d\Phi\,e^{-(2R/l)+nS_0}\approx\beta_0\ln\left(\frac{C}{2\beta_0}\right), \tag{6}$$

where C is a constant of the order of unity. Thus, for $B=0$ the "empty corridor" effect simply changes the constant in the argument of the logarithm.

The key idea suggested in Ref. 16 was that for $B\neq 0$ the area of the overlap of the two corridors, S_B, sharply depends

on B, resulting in the observed MR. Indeed, it is seen from Fig. 1(b) that for $\beta \gtrsim \beta_0$, $S_B \to 0$, resulting in sharp negative MR,

$$\frac{\delta\rho_{xx}}{\rho} \sim \int_0^\infty \frac{dR}{l} \int_0^{a/R} d\phi\, e^{-2R/l}(e^{nS_B} - e^{nS_0}). \tag{7}$$

The following qualitative explanation of the observed linear MR was presented in Ref. 16. The value $n(S_B - S_0)$ was estimated for $\phi = 0$ [see Fig. 1(c)] to the first order in B as $-nR^3/R_c = -R^3/2alR_c$, where R_c is the cyclotron radius. Assuming that this estimate also works at $\phi \neq 0$ and expanding $e^{nS_B} - e^{nS_0}$ to the first order in B, one gets $\delta\rho_{xx}/\rho \sim -l/R_c = -\omega_c\tau$.

In fact, the physical picture of the phenomenon is more subtle. The contribution of any trajectory with $\phi \neq 0$ is cancelled to the first order in B by the contribution of the time-reversed trajectory, since the values of $S_B - S_0$ are opposite for these paths [see Figs. 1(d) and 1(e)]. The cancellation does not occur only at very small $\phi \sim \beta$. The integration in Eq. (7) over $\phi < \beta$ yields $\delta\rho_{xx}/\rho \sim -\beta^2/\beta_0$. Larger values of ϕ also give a quadratic in β contribution to the MR. This contribution is positive and comes from the second order term in the expansion of $e^{nS_B} - e^{nS_0}$ in B. It follows from our results [see Eqs. (1) and (62)] that the contribution of small angles is dominant resulting in a negative parabolic MR. We find that the parabolic MR crosses over to linear at very small $\beta \approx 0.05\beta_0$, which explains why the parabolic MR was not seen in numerical simulations[16] and experiment.[18] Note that for very small $\beta < \beta_0^2$ contribution of the trajectories with a long Lyaponov region (Lyapunov trajectories) becomes important. In the Sec. III we focus on the region $\beta > \beta_0^2$ where the contribution of the Lyapunov trajectories is parametrically small. The Lyapunov trajectories will be discussed in Sec. IV.

III. CALCULATIONS

A. Kinetic equation

In this section we introduce the kinetic equation which is the starting point for the calculation of the diffusion coefficient and the resistivity of the Lorenz gas.

We consider the Lorenz gas at zero temperature, assuming that the electrons participating in the conduction have the Fermi velocity v_F. The diffusion coefficient D is given by

$$D = \frac{1}{2}\int_0^\infty dt \langle \mathbf{v}(0)\mathbf{v}(t)\rangle = \frac{1}{2}\int_{-\infty}^\infty dt \int d\mathbf{r}\, d\mathbf{v} \langle G_R\rangle \mathbf{v}\mathbf{v}_0. \tag{8}$$

Here $G_R = G_R(\mathbf{v}, \mathbf{v}_0, \mathbf{r}, \mathbf{r}_0, t)$ is the retarded Green's function of the Liouville equation and $\langle \cdots \rangle$ stands for the averaging over the positions of the disks.[24] The equation for G_R reads

$$\left(\frac{\partial}{\partial t} + \mathbf{v}\frac{\partial}{\partial \mathbf{r}} - \omega_c\left[\mathbf{v} \times \frac{\partial}{\partial \mathbf{v}}\right] - \hat{T}\right) G_R = \delta(\mathbf{r} - \mathbf{r}_0)\delta(\mathbf{v} - \mathbf{v}_0)\delta(t), \tag{9}$$

$$G_R = 0 \quad \text{for } t < 0,$$

where $\mathbf{v}\partial/\partial\mathbf{r} - \omega_c[\mathbf{v} \times \partial/\partial\mathbf{v}]$ is the Liouville operator of the free motion in the magnetic field and $\hat{T}$ describes scattering on the disks. From Eq. (8) it follows that we need the time integral of G_R rather than the whole time-dependent function. This integral can be written as

$$\int_0^\infty dt\, G_R(\mathbf{v}, \mathbf{v}_0, \mathbf{r}, \mathbf{r}_0, t) = \frac{\delta(v - v_F)}{v_F} G_{\alpha,\alpha_0}(\mathbf{r}, \mathbf{r}_0), \tag{10}$$

where α, α_0 are the angles of velocities $\mathbf{v}$ and $\mathbf{v}_0$, respectively. Here we used the energy conservation, which implies that in scattering processes the absolute value of the velocity does not change. Using Eq. (10), the diffusion coefficient Eq. (8) can be rewritten as

$$D = \frac{v_F}{4\pi \mathrm{S}} \int d\mathbf{r}\, d\mathbf{r}_0\, d\alpha\, d\alpha_0 \langle G_{\alpha,\alpha_0}(\mathbf{r}, \mathbf{r}_0)\rangle \cos(\alpha - \alpha_0). \tag{11}$$

Since $\langle G_{\alpha,\alpha_0}(\mathbf{r}, \mathbf{r}_0)\rangle$ depends on $\alpha - \alpha_0$ and $\mathbf{r} - \mathbf{r}_0$ only, it is convenient to average over the position of the initial point and over the initial angle. Here S is the area of the sample. Integrating Eq. (9) with respect to time the equation for $G = G_{\alpha,\alpha_0}(\mathbf{r}, \mathbf{r}_0)$ is written as

$$(\epsilon + \hat{L}_0 - \hat{T}_- - \hat{T}_+)G = \delta(\mathbf{r} - \mathbf{r}_0)\delta(\alpha - \alpha_0), \tag{12}$$

where

$$\hat{L}_0 = \mathbf{n}\frac{\partial}{\partial \mathbf{r}} - \frac{1}{R_c}\frac{\partial}{\partial \alpha},$$

$\mathbf{n} = \cos\alpha \mathbf{e}_x + \sin\alpha \mathbf{e}_y$ is the unit vector in the direction of $\mathbf{v}$ and $\epsilon \to 0$. The interaction with disks is written in Eq. (12) in the form of collision integral.[20,25] The scattering operators $\hat{T}^\pm$ transform arbitrary function $f(\mathbf{r}, \alpha)$ as follows:

$$\hat{T}^+ f(\mathbf{r}, \alpha) = \int d\alpha' \sigma(\alpha - \alpha') n^+ f(\mathbf{r}, \alpha'),$$

$$\hat{T}^- f(\mathbf{r}, \alpha) = -f(\mathbf{r}, \alpha) \int d\alpha'\, \sigma(\alpha - \alpha') n^-, \tag{13}$$

where

$$n^\pm = n^\pm(\mathbf{r}, \mathbf{a}) = \sum_i \delta(\mathbf{r} - \mathbf{R}_i \pm \mathbf{a}). \tag{14}$$

Here $\mathbf{R}_i$ are the positions of the disk's centers and

$$\sigma(\varphi) = \frac{a}{2}\left|\sin\frac{\varphi}{2}\right| \tag{15}$$

is the differential cross section of one disk. The vector $\mathbf{a}$ depends on angles α, α' in the integrals Eq. (13),

$$\mathbf{a} = \mathbf{a}_{\alpha,\alpha'} = \frac{(\mathbf{n}' - \mathbf{n})a}{\sqrt{2(1 - \mathbf{n}'\mathbf{n})}}, \tag{16}$$

and is pointing from the center of a disk to the scattering point at the disk surface (see Fig. 2). Physically, operator $\hat{T}^+$

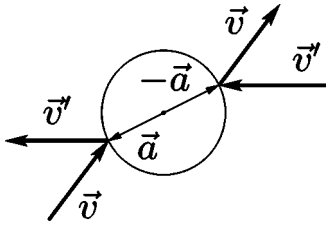

FIG. 2. Scattering of a particle on a hard disk.

describes influx of particles to velocity $\mathbf{v}$ at the point $\mathbf{R}_i-\mathbf{a}$, while operator $\hat{T}^-$ describes the outflux from velocity $\mathbf{v}$ at the point $\mathbf{R}_i+\mathbf{a}$. The averaged value of the $n^{\pm}$ is equal to the disks concentartion

$$\langle n^+\rangle = \langle n^-\rangle = n. \tag{17}$$

The Boltzmann equation is obtained by averaging the Liouville equation with respect to the position of the scatterers and neglecting correlations. Indeed, using Eq. (17) one finds that the average collision operators Eq. (13) are given by

$$\langle \hat{T}^+\rangle f(\mathbf{r},\alpha) = n\int d\alpha'\ \sigma(\alpha-\alpha')f(\mathbf{r},\alpha'),$$

$$\langle \hat{T}^-\rangle = -n\int d\alpha'\ \sigma(\alpha-\alpha') = -1/l. \tag{18}$$

Replacing the collision operators in the Liouville equation Eq. (12) with their averages Eq. (18) one obtains the Boltzmann equation

$$\hat{L}_0 G^B_{\alpha,\alpha_0}(\mathbf{r}) - n\int d\alpha'\ \sigma(\alpha-\alpha')(G^B_{\alpha',\alpha_0}(\mathbf{r}) - G^B_{\alpha,\alpha_0}(\mathbf{r})) = \delta(\mathbf{r})\delta(\alpha-\alpha_0). \tag{19}$$

The Boltzmann-Drude diffusion coefficient D_0 in the absence of the magnetic field is found from Eqs. (19) and (11) as follows. Integrating (19) with respect to $\mathbf{r}$ and expanding the Green's function G^B in angular harmonics one finds

$$\int G^B_{\alpha,\alpha_0}(\mathbf{r})d\mathbf{r} = \frac{1}{2\pi}\sum_m l_m e^{im(\alpha-\alpha_0)}, \tag{20}$$

where

$$l_m^{-1} = n\int d\varphi\ \sigma(\varphi)(1-\cos(m\varphi)). \tag{21}$$

In particular,

$$l_1 = l_{\mathrm{tr}} = \frac{3l}{4} = \frac{3}{8na} \tag{22}$$

is the transport length. Substituting Eqs. (20) and (22) in Eq. (11) one finds

$$D_0 = \frac{v_F l_{\mathrm{tr}}}{2}. \tag{23}$$

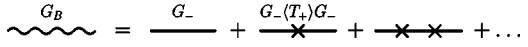

FIG. 3. Expansion of Boltzmann propagator G^B in a series in ballistic propagators G.

B. Perturbative expansion

In this section we derive the perturbative expansion for the average Green's function in order to take into account non-Markovian corrections which are absent in the Boltzmann-Drude picture.

Introduce the operators

$$\delta\hat{T}^{\pm} = \hat{T}^{\pm} - \langle \hat{T}^{\pm}\rangle \tag{24}$$

which describe the fluctuation of the collision integral with respect to its average value. Using these operators the formal solution of (12), $\hat{G}=(\epsilon+\hat{L}_0-\hat{T}^- - \hat{T}^+)^{-1}$ can be written as the following series:

$$\langle \hat{G}\rangle = \hat{G}^B + \sum_{\mu,\nu=\pm}\hat{G}^B\langle \delta\hat{T}^{\mu}\hat{G}^B\delta\hat{T}^{\nu}\rangle\hat{G}^B + \cdots, \tag{25}$$

where G^B is defined by Eq. (19). Here we took into account that $\langle\delta\hat{T}\rangle=0$. The first term on the right-hand side of Eq. (25) gives the Drude-Boltzmann result described in the preceding section. The rest of the terms in Eq. (25) provide a regular way for the calculation of correlations, which are absent in the Boltzmann picture.

In the subsequent analysis of the perturbative expansion Eq. (25) we will extensively use the representation of the Boltzmann propagator G_B in terms of the ballistic propagator

$$\hat{G}^- = (\hat{L}_0 + 1/l)^{-1}. \tag{26}$$

This is achieved by expanding the Boltzmann propagator $G^B=(L_0+1/l-\langle\hat{T}^+\rangle)^{-1}$ as a sum over the number of scattering events represented by the operator $\langle\hat{T}^+\rangle$,

$$G^B = G^- + G^-\langle\hat{T}^+\rangle G^- + \cdots. \tag{27}$$

The diagrammatic representation of the expansion (27) is shown in Fig. 3. Each cross in this figure corresponds to $\langle\hat{T}^+\rangle$ and each solid line to a ballistic propagator G^-. For future reference we write the explicit expression for the ballistic Green's function in zero magnetic field and in weak magnetic fields. For $B=0$ the ballistic propagator conserves the velocity. In this case its kernel is given by

$$G^-_{\alpha,\alpha_0}(\mathbf{r}) = \delta(\alpha-\alpha_0)\delta(\alpha_0-\alpha[\mathbf{r}])\frac{\exp(-r/l)}{r}. \tag{28}$$

Here $\alpha[\mathbf{r}]$ is the angle of the vector $\mathbf{r}$. Magnetic field rotates the velocity vector with the cyclotron frequency. For small magnetic fields, $\beta\ll 1$, we have

$$G^-_{\alpha,\alpha_0}(\mathbf{r}) \approx \delta(\alpha-\alpha[\mathbf{r}]-r/2R_c) \times \delta(\alpha_0-\alpha[\mathbf{r}]+r/2R_c)\frac{\exp(-r/l)}{r}. \tag{29}$$

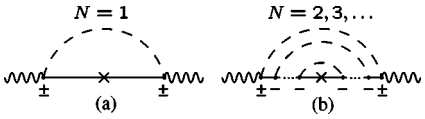

FIG. 4. Diagrams, corresponding to the process shown in Fig. 1(a). Diagram (a) does not take into account the "empty corridor" effect and should be renormalized by diagrams (b).

C. Ballistic returns in perturbative expansion

In this section we show how the processes of ballistic returns discussed in Sec. II arise in the perturbative expansion Eq. (27). Consider the second term in Eq. (25). This term describes the memory effect due to diffusive returns. As discussed in Sec. II, the main contribution comes from returns after a single scattering. This process is described by the diagram shown in Fig. 4(a). The dashed line corresponds to the pairings $\langle \delta\hat{T}^{\mu}\delta\hat{T}^{\nu}\rangle$ $(\mu,\nu=\pm)$, external wavy lines to the diffusion propagators $\hat{G}^{B}$. The internal line corresponds to the Boltzmann propagator Eq. (27) truncated at one scattering $\hat{G}^{-}\langle\hat{T}^{+}\rangle\hat{G}^{-}$.

Four combinations of $(\pm,\pm)$ at the ends of external dashed lines in the diagrams shown in Fig. 4(a) represent four different types of correlation at a given point **R**. To see this consider the pairing $\langle \delta\hat{T}^{\mu}\delta\hat{T}^{\nu}\rangle$. By virtue of Eqs. (13) and (14) this pairing is proportional to the density-density correlation function $\langle (n^{\mu}(\mathbf{r}_1,\mathbf{a}_1)-n)(n^{\nu}(\mathbf{r}_2,\mathbf{a}_2)-n)\rangle$ for $\mu=\pm$, $\nu=\pm$. Assuming that disks are randomly distributed over the sample we get for these functions

$$\langle (n^{\mu}(\mathbf{r}_1,\mathbf{a}_1)-n)(n^{\nu}(\mathbf{r}_2,\mathbf{a}_2)-n)\rangle = n\int d\mathbf{R}\;\delta(\mathbf{r}_2-\mathbf{R}+\mu\mathbf{a}_1)\delta(\mathbf{r}_1-\mathbf{R}+\nu\mathbf{a}_2). \quad (30)$$

It is natural to interpret the vector **R** as the position of the center of the disk on which a double scattering occurs. However, this interpretation is valid for diagram $(+,+)$ only. As shown in Fig. 5, this diagram corresponds to the situation where an electron experiences two real scattering processes on the disk placed at point **R**. The physical interpretation of other diagrams is more subtle. The diagram $(-,-)$ (see Fig. 6) does not correspond to any real scattering at point **R**. It just allows one to calculate correctly the probability for an electron to pass twice the region of the size a around point **R**

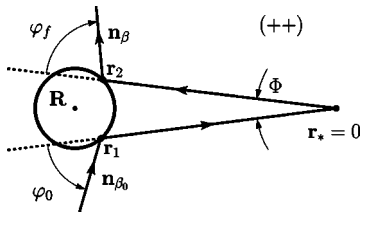

FIG. 5. Electron trajectory related to the pairing $(+,+)$. An electron scatters twice (at points $\mathbf{r}_1$ and $\mathbf{r}_2$) on the surface of a disk, placed at point **R**. For a fixed position of the backscattering point $(\mathbf{r}_*=0)$, the process is parametrized by **R**, and by the scattering angles φ_0, φ_f.

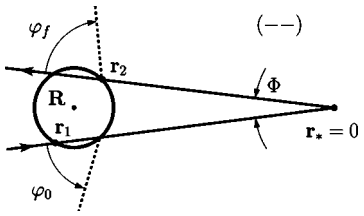

FIG. 6. Electron trajectory for the $(-,-)$ pairing. Electron does not experience any real scattering except as scattering at $\mathbf{r}_*=0$. The diagram $(-,-)$ gives the probability to pass twice the region around point **R** without scattering.

without scattering. To interpret the diagrams $(+,-)$ and $(-,+)$, note that in the Boltzmann picture, which neglects correlations, the following process is allowed. An electron scatters on a disk and later on passes through the region occupied by this disk without a scattering (see Fig. 7) (analogous consideration is valid for diagram shown in Fig. 8). The diagrams $(+,-)$ and $(-,+)$ correct the Boltzmann result by subtracting the contribution of such unphysical processes.

As follows from the qualitative discussion Sec. II, the processes of ballistic returns after a single scattering give rise to the leading (nonanalytic) correction to the Drude-Boltzmann result in zero magnetic field. However, taking into account diagrams shown in Fig. 4(a) (describing processes shown in Figs. 5–8) is not sufficient for calculation of the low field anomaly of the MR. Actually, diagrams in Fig. 4(a) do not contain the "empty corridor" effect. We will show that the correct description of the memory effects, specific for ballistic returns, requires the renormalization of diagrams 4(a) by diagrams 4(b), in which the internal dashed lines contains $(-,-)$ pairings only. Physically, the Nth order diagram of the type 4(b) represents the $N-1$th order term in the Taylor expansion of the $\exp(-nS_0)$ in the qualitative estimate (6). Such renormalization play the key role in the quantitative description of the anomalous MR.

In the next section we derive the analytical expression for diagrams 4(a). Then we generalize the calculations to account for the corridor effect and calculation of anomalous MR.

D. Nonanalytical corrections to the zero-field resistance neglecting the "empty corridor" effect

In this section we use the perturbative expansion Eq. (25) to derive analytically the leading correction to the diffusion coefficient. This correction is due to the processes described

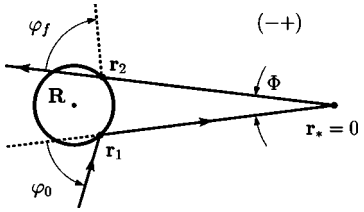

FIG. 7. "Unphysical" electron trajectory related to the pairing $(-,+)$: electron scatters on a disk and after a while passes the region occupied by this disk without scattering.

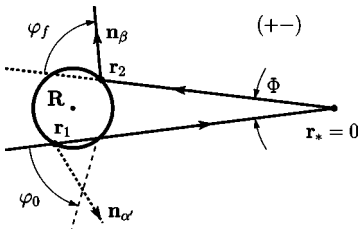

FIG. 8. "Unphysical" electron trajectory related to the pairing $(+,-)$: electron passes the region occupied by a disk without scattering and later on scatters on this disk. The diagram related to such trajectory corrects the Boltzmann result by subtracting the probability of this unphysical event. It is convenient to parametrize this trajectory by the scattering angles for the $(+,+)$ process.

by diagram Fig. 4(a). The operator expression of the correction to the Green's function related to this diagram is given by

$$\sum_{\mu,\nu=\pm} \hat{G}^B \underbrace{\delta\hat{T}^\mu \hat{G}^- \langle \hat{T}^+ \rangle \hat{G}^- \delta\hat{T}^\nu} \hat{G}^B,$$

where the underbracket stands for the pairings of operators $\delta\hat{T}^\mu$ and $\delta\hat{T}^\nu$. Substituting this correction into Eq. (11), and using Eqs. (20) and (21) to integrate over $\mathbf{r}$, $\mathbf{r}_0$, α, α_0 we get

$$\delta D = \frac{v_F l_{\rm tr}^2}{4\pi} \int d\beta_0\, d\beta\, M_{\beta,\beta_0} \cos(\beta - \beta_0), \tag{31}$$

where

$$M_{\beta,\beta_0} = \frac{1}{S} \sum_{\mu,\nu=\pm} \int d\mathbf{r}_*\, d\mathbf{r}_1\, d\mathbf{r}_2\, d\alpha_1\, d\alpha_2\, d\beta_1\, d\beta_2 \times \langle \delta T^\mu_{\beta,\alpha_2}(\mathbf{r}_2) G^-_{\alpha_2,\beta_2}(\mathbf{r}_2 - \mathbf{r}_*) n\sigma(\beta_2 - \beta_1) \times G^-_{\beta_1,\alpha_1}(\mathbf{r}_* - \mathbf{r}_1)\, \delta T^\nu_{\alpha_1,\beta_0}(\mathbf{r}_1) \rangle. \tag{32}$$

Here we used Eq. (18) for $\langle \hat{T}^+ \rangle$. Graphically, these calculations are presented in Fig. 9. The pairings $\langle \delta T^\mu_{\beta,\alpha_2}(\mathbf{r}_2)\, \delta T^\nu_{\alpha_1,\beta_0}(\mathbf{r}_1) \rangle$, entering Eq. (32), are given in Appendix A for four possible combinations of μ, ν. The pairings only depend on the difference $\mathbf{r}_1 - \mathbf{r}_2$. Therefore in Eq. (32) one can remove the integral over $\mathbf{r}_*$ and the sample area S in the denominator and set $\mathbf{r}_* = 0$ in the integrand. In other words we set the origin of the coordinate system at the backscattering point $\mathbf{r}_*$. Next we integrate Eq. (32) over the angles α_1, α_2, β_1, β_2. This integration can be easily done taking into account angle dependent delta functions entering in $G^-_{\alpha_2,\beta_2}(\mathbf{r}_2)$ and $G^-_{\beta_1,\alpha_1}(-\mathbf{r}_1)$ [see Eq. (28)]. As a result we get $\alpha_1 = \beta_1 = \alpha[-\mathbf{r}_1]$, $\alpha_2 = \beta_2 = \alpha[\mathbf{r}_2]$, and

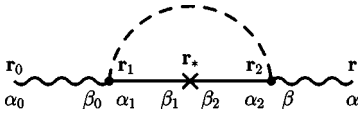

FIG. 9. Graphical representation of Eqs. (31) and (32).

$$M_{\beta,\beta_0} \approx n\sigma(\pi) \sum_{\mu,\nu=\pm} \int d\mathbf{r}_1\, d\mathbf{r}_2 \times \langle \delta T^\mu_{\beta,\alpha[\mathbf{r}_2]}(\mathbf{r}_2)\, \delta T^\nu_{\alpha[-\mathbf{r}_1],\beta_0}(\mathbf{r}_1) \rangle \frac{e^{-r_2/l} e^{-r_1/l}}{r_2 r_1}. \tag{33}$$

In derivation of Eq. (33) we took into account that the pairing of collision operators $\langle \delta T^\mu(\mathbf{r}_1)\, \delta T^\nu(\mathbf{r}_2) \rangle$ vanishes for $|\mathbf{r}_1 - \mathbf{r}_2| > 2a$, which is clear from its physical meaning and also can be seen from the delta functions in the factor $J(\mathbf{a},\mathbf{b})$ (see Appendix A). At the same time both r_1 and r_2 are of the order of the mean free path $l \gg a$. Therefore, $\beta_2 - \beta_1 = \alpha[\mathbf{r}_2] - \alpha[-\mathbf{r}_1] \approx \pi$, and $\sigma(\beta_2 - \beta_1) \approx \pi$. Physically this means that the typical scattering angle in the processes of ballistic return are close to π. Next, we use Eq. (33) to evaluate the contributions of different pairings μ, ν.

$(+,+)$ *pairing*: Consider first the process in which $\mu = +$, $\nu = +$. Substitute Eqs. (A3) and (33) in Eq. (31) and integrate over $\mathbf{r}_1$, $\mathbf{r}_2$. It is convenient for our purposes to perform this integration for a fixed value of the vector $\mathbf{R}$. Then the delta functions in Eq. (A7) ensure that $\mathbf{r}_1$ and $\mathbf{r}_2$ lie on the circle of the radius a centered in the point $\mathbf{R}$,

$$\mathbf{r}_1 = \mathbf{R} - \mathbf{a}_{\alpha[-\mathbf{r}_1],\beta_0}, \quad \mathbf{r}_2 = \mathbf{R} - \mathbf{a}_{\beta,\alpha[\mathbf{r}_2]}. \tag{34}$$

The graphical solution of these equations is shown in Fig. 5 (vectors $\mathbf{n}_\beta$,$\mathbf{n}_{\beta_0}$ in this figure are the unit vectors in the directions of β and β_0, respectively). Since a is small ($a \ll l$) one has approximately

$$\mathbf{r}_1 \approx \mathbf{r}_2 \approx \mathbf{R}. \tag{35}$$

This accuracy is sufficient for the calculation of the diagram in Fig. 4(a) (since we calculate it in the lowest order in a/l). Upon integrating out the vectors $\mathbf{r}_1$, $\mathbf{r}_2$ the integrand in Eq. (31) depends on $\mathbf{R}$. Finally we get

$$\delta D^{++} = \frac{v_F l_{\rm tr}^2 n^2 \sigma(\pi)}{4\pi} \int d\mathbf{R}\, d\beta\, d\beta_0 \cos(\beta - \beta_0) \times \sigma(\beta - \alpha[\mathbf{R}]) \sigma(\alpha[-\mathbf{R}] - \beta_0) \frac{e^{-2R/l}}{R^2}. \tag{36}$$

Introducing new variables $\varphi_0 = \beta_0 - \alpha[-\mathbf{R}]$ and $\varphi_f = \alpha[\mathbf{R}] - \beta$ and taking into account that $\alpha[\mathbf{R}] = \alpha[-\mathbf{R}] + \pi$ and $\sigma(-\varphi) = \sigma(\varphi)$, the relative correction to the diffusion coefficient is written as

$$\frac{\delta D^{++}}{D_0} = -\frac{n l_{\rm tr}}{4l} \int \frac{dR}{R} d\varphi_0\, d\varphi_f\, e^{-2R/l} \times \sigma(\varphi_f) \sigma(\varphi_0) \cos(\varphi_0 + \varphi_f). \tag{37}$$

From Fig. 5 it is seen that φ_0, φ_f are the scattering angles.

$(+,-)$ *pairing*: Next we present calculations for $\mu = +$, $\nu = -$. Like the calculation of the diagram $(+,+)$, we substitute Eq. (33) and Eq. (A5) into Eq. (31) and integrate over $\mathbf{r}_1$, $\mathbf{r}_2$ with the use of Eq. (A7). The values of $\mathbf{r}_1$ and $\mathbf{r}_2$ should be found from the following equations:

$$\mathbf{r}_1 = \mathbf{R} + \mathbf{a}_{\alpha[-\mathbf{r}_1],\alpha'}, \quad \mathbf{r}_2 = \mathbf{R} - \mathbf{a}_{\beta,\alpha[\mathbf{r}_2]}. \tag{38}$$

The graphical solution of these equation is presented in Fig. 8. After integrating out vectors $\mathbf{r}_1$, $\mathbf{r}_2$ and the angle β_0 we get

$$\delta D^{+-} = -\frac{v_F l_{\rm tr}^2 n^2 \sigma(\pi)}{4\pi} \int d\mathbf{R}\, d\beta\, d\alpha' \cos(\beta - \alpha[-\mathbf{R}]) \times \sigma(\beta - \alpha[\mathbf{R}])\sigma(\alpha[-\mathbf{R}] - \alpha')\frac{e^{-2R/l}}{R^2}. \tag{39}$$

In derivation of this equation we have used Eq. (35). It is convenient to rewrite this equation using as integration variables φ_0, φ_f, which are the scattering angles for the process $(+,+)$. They are expressed in terms of α' and β as $\varphi_0 = \alpha[-\mathbf{R}] - \alpha'$, $\varphi_f = \alpha[\mathbf{R}] - \beta$. In these variables Eq. (39) reads

$$\frac{\delta D^{+-}}{D_0} = \frac{n l_{\rm tr}}{4l} \int \frac{dR}{R} d\varphi_0\, d\varphi_f\, e^{-2R/l} \sigma(\varphi_f)\sigma(\varphi_0)\cos(\varphi_f). \tag{40}$$

It is seen from Eq. (40) (see also Fig. 8) that the contribution of the process $(+,-)$ can be parametrized by the angles φ_0 and φ_f, which are the scattering angles for the process $(+,+)$. Analogous calculations can be easily done for other types of correlations.

Summing the different contributions $\delta D = \delta D^{++} + \delta D^{+-} + \delta D^{-+} + \delta D^{--}$ we get the following expression for the diagram Fig. 4(a):

$$\frac{\delta\rho}{\rho} = -\frac{\delta D}{D} = \frac{n l_{\rm tr}}{4l} \mathrm{Re} \int_a^\infty \frac{dR}{R} e^{-2R/l} \int_0^{2\pi} d\varphi_0 \int_0^{2\pi} d\varphi_f\, \sigma(\varphi_0)\sigma(\varphi_f) \times (1 - e^{i\varphi_0})(1 - e^{i\varphi_f}) = \frac{2\beta_0}{3} \ln\left(\frac{1}{2\beta_0}\right). \tag{41}$$

This equation is the exact expression for the nonanalytic correction[19–23] to the Drude-Boltzmann resistivity which was qualitatively given in Eq. (3). Four terms in the product $(1 - e^{i\varphi_0})(1 - e^{i\varphi_f}) = 1 - e^{i\varphi_0} - e^{i\varphi_f} + e^{i(\varphi_0 + \varphi_f)}$ correspond to four types of correlations discussed above.

E. "Empty corridor" effects on the zero-field resistance

In this section we use the perturbation theory for the quantitative derivation of the effect of the "empty corridor" discussed in Sec. II.

Equation (41) takes into account one pairing of operators $\delta\hat{T}^{\mu}$ and $\delta\hat{T}^{\nu}$. The terms containing N pairings (N dashed lines) are typically small as β_0^N. However, there is a series of diagrams, shown in Fig. 4(b), whose contribution is of the order β_0 (see Ref. 21). The internal dashed lines in this series only contain pairings $\langle \delta\hat{T}^{-}\delta\hat{T}^{-}\rangle$. Below we show that the series Fig. 4(b) accounts for the effect of the "empty corridor." More precisely, we prove that the Nth order term in this series corresponds to $N-1$ term in the Taylor expansion of the $\exp(nS_0)$ in Eq. (4).

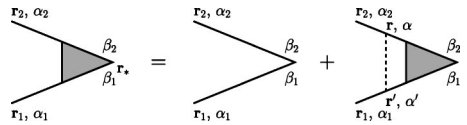

FIG. 10. Dyson equation, describing the renormalization of backscattering events by the "empty corridor" effect. Nth order term in the these stairlike diagrams corresponds to the $(N-1)$th term in the Taylor expansion of $\exp(nS_0)$ in Eq. (4).

The addition of the diagram Fig. 4(b) to the diagram Fig. 4(a) leads to following replacement in Eq. (32),

$$G^{-}_{\alpha_2,\beta_2}(\mathbf{r}_2) G^{-}_{\beta_1,\alpha_1}(-\mathbf{r}_1) \to K^{\alpha_1,\alpha_2}_{\beta_1,\beta_2}(\mathbf{r}_1,\mathbf{r}_2), \tag{42}$$

where the function $K^{\alpha_1,\alpha_2}_{\beta_1,\beta_2}(\mathbf{r}_1,\mathbf{r}_2)$ can be found from the Dyson equation (see Fig. 10). Since the operator $\delta\hat{T}^{-}$ does not change the velocity angle, one can search the solution of the Dyson equation in the form

$$K^{\alpha_1,\alpha_2}_{\beta_1,\beta_2}(\mathbf{r}_1,\mathbf{r}_2) = G^{-}_{\alpha_2,\beta_2}(\mathbf{r}_2) G^{-}_{\beta_1,\alpha_1}(-\mathbf{r}_1)\Gamma(r_1,r_2,\Phi), \tag{43}$$

where Φ is the difference between the backscattering angle and π (see Fig. 11). While substituting Eq. (43) in the Dyson equation (which is shown graphically in Fig. 10), integrating over angles α, α', and using the identity

$$\delta(\alpha[\mathbf{r}_2 - \mathbf{r}] - \alpha[\mathbf{r}]) = \frac{|\mathbf{r}_2 - \mathbf{r}|}{r_2}\delta(\alpha[\mathbf{r}] - \alpha[\mathbf{r}_2])\,\theta(r_2 - r) \tag{44}$$

(and analogous identity for vectors $\mathbf{r}', \mathbf{r}_1$) we get

$$\Gamma(r_1,r_2,\Phi) = 1 + \int_{r<r_2}\int_{r'<r_1} d\mathbf{r}\, d\mathbf{r}' \times \frac{\delta(\alpha[\mathbf{r}] - \alpha[\mathbf{r}_2])\,\delta(\alpha[-\mathbf{r}'] - \alpha[-\mathbf{r}_1])}{rr'} \times \langle \delta T^{-}_{\alpha[\mathbf{r}_2]}(\mathbf{r})\, \delta T^{-}_{\alpha[-\mathbf{r}_1]}(\mathbf{r}')\rangle \Gamma(r,r',\Phi), \tag{45}$$

where $\delta T^{-}_{\alpha}(\mathbf{r})$ are defined in Appendix A. Further calculations can be done in two different ways. It is useful from methodological point of view to discuss both of them. One way is to first integrate Eq. (46) over the angles of the vectors $\mathbf{r}$ and $\mathbf{r}'$ (see Fig. 10). The delta functions entering in Eq. (46) ensure that point $\mathbf{r}$ (see Figs. 10 and 11) lies on the line segment connecting point $\mathbf{r}_1$ and the origin and point $\mathbf{r}'$ lies on the line segment connecting point $\mathbf{r}_2$ and the origin. This allows to reduce the Dyson equation to the closed relation for function $\Gamma(r_1,r_2,\Phi)$,

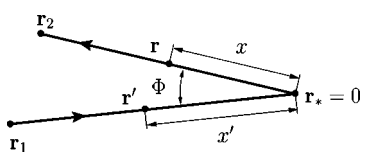

FIG. 11. Pairings $\langle \delta\hat{T}^{-}\delta\hat{T}^{-}\rangle$ do not change the electron trajectory. Point $\mathbf{r}$ (see Fig. 10) lies on the line segment connecting point $\mathbf{r}_1$ and the origin and point $\mathbf{r}'$ lies on the line segment connecting point $\mathbf{r}_2$ and the origin.

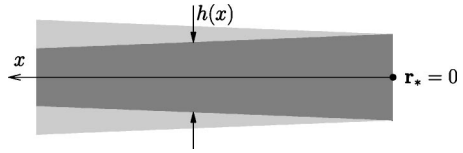

FIG. 12. Width of the overlap region as a function of a distance from the origin.

$$\Gamma(r_1,r_2,\Phi) = 1 + \int_0^{r_1} dr' \int_0^{r_2} dr \langle \delta T^{-}_{\alpha[\mathbf{r}_2]}(\mathbf{r}) \times \delta T^{-}_{\alpha[-\mathbf{r}_1]}(\mathbf{r}') \rangle \Gamma(r,r',\Phi), \tag{46}$$

where the pairing

$$\langle \delta T^{-}_{\alpha[\mathbf{r}_2]}(\mathbf{r})\, \delta T^{-}_{\alpha[-\mathbf{r}_1]}(\mathbf{r}') \rangle \approx h(r,\Phi)\,\delta(r-r'), \tag{47}$$

is calculated in Appendix B. Here

$$h(r,\Phi) = (2a - |\Phi| r)\,\theta(2a - |\Phi| r) \tag{48}$$

is shown in Fig. 12. As a result we have

$$\Gamma(r_1,r_2,\Phi) = 1 + n \int_0^{\min[r_1,r_2]} dr\, h(r,\Phi)\Gamma(r,r,\Phi). \tag{49}$$

This equation has an evident solution

$$\Gamma(r_1,r_2,\Phi) = \exp\left(n \int_0^{\min[r_1,r_2]} dr\, h(r,\Phi) \right). \tag{50}$$

Equation (50) may be derived in an alternative way. This way allows to understand on the formal basis why one should renormalize the diagrams in Fig. 4(a) by the $\langle \delta\hat{T}^{-} \delta\hat{T}^{-} \rangle$ pairings only. Let us integrate in Eq. (46) over $\mathbf{r},\mathbf{r}'$, using Eq. (A4). Doing this, we get

$$\Gamma(r_1,r_2,\Phi) = 1 + n \int d\alpha'\, d\alpha'' \int_{R<\min[r_1,r_2]} d\mathbf{R} \frac{\delta(\alpha[\mathbf{R} + \mathbf{a}_{\alpha[\mathbf{r}_2],\alpha'}] - \alpha[\mathbf{r}_2])\,\delta(\alpha[-\mathbf{R} - \mathbf{a}_{\alpha[-\mathbf{r}_1],\alpha''}] - \alpha[-\mathbf{r}_1])}{R^2} \times \sigma(\alpha[\mathbf{r}_2] - \alpha')\sigma(\alpha[\mathbf{r}_1] - \alpha'')\Gamma(R,R,\Phi). \tag{51}$$

Here we took into account that $\Gamma(r,r',\Phi)$ is a slowly changing function of r,r' (it changes on a scale of the order of l). Since Eq. (A4) provides $|\mathbf{r}-\mathbf{R}| \sim |\mathbf{r}'-\mathbf{R}| \sim a$, we set $\Gamma(r,r',\Phi) \approx \Gamma(R,R,\Phi)$. Next we make use of the identity

$$\int d\alpha'\, \sigma(\alpha-\alpha')\,\delta(\alpha[\mathbf{R} + \mathbf{a}_{\alpha,\alpha'}] - \alpha) \approx R\,\theta(a/R - |\alpha - \alpha[\mathbf{R}]|) \tag{52}$$

to integrate over α',α''. After this integration we get

$$\Gamma(r_1,r_2,\Phi) = 1 + n \int_0^{\min[r_1,r_2]} R\, dR\, d\alpha[\mathbf{R}] \times \theta(a/R - |\alpha[\mathbf{r}_2] - \alpha[\mathbf{R}]|) \times \theta(a/R - |\alpha[\mathbf{r}_1] - \alpha[\mathbf{R}]|)\Gamma(R,R',\Phi). \tag{53}$$

Integration over $\alpha[\mathbf{R}]$ leads again to Eq. (50).

From Eq. (35) it follows that we need to know Γ for $r_1 \approx r_2 \approx R$. Using Eq. (50) we find

$$\Gamma(R,R,\Phi) = \exp\left(n \int_0^R dr\, h(r,\Phi) \right) = e^{nS_0(R,\Phi)}, \tag{54}$$

where $S_0(R,\Phi)$ is the overlap between two corridors, given by Eq. (5). The nth order term in the Taylor expansion of the exponential (54) corresponds to a diagram in Fig. 4(b) with $n+1$ dashed lines. Indeed, the nth order term in the Taylor expansion contains n integration over coordinates of n scatterings of the type $-$, $-$. What remains to do to get the resistivity correction is to express Φ in Eq. (54) via angles φ_0,φ_f. To do this, the precision Eq. (35) is not sufficient. More specifically, we will need to know the angle between vectors $\mathbf{r}_1$ and $\mathbf{r}_2$ to the order a/l. For this purpose it will be sufficient to make replacements $\alpha[-\mathbf{r}_1] \approx \alpha[-\mathbf{R}]$ and $\alpha[\mathbf{r}_2] \approx \alpha[\mathbf{R}]$ in the arguments of vectors $\mathbf{a}$ in Eq. (34). Then the angle Φ is calculated as (see Figs. 5–8)

$$\Phi \approx \frac{a}{R}[\cos(\varphi_0/2) + \cos(\varphi_f/2)]. \tag{55}$$

This equation is valid for $0 < \varphi_0 < 2\pi$, $0 < \varphi_f < 2\pi$ [since $\cos(\varphi/2)$ is not periodic with 2π one should specify the integration limits]. It worth noting that Eq. (55) ensures that the argument of the θ function in Eq. (48) is positive and the overlap width and overlap area are given by

$$h(r,\Phi) = 2a - |\Phi| r,$$

$$S_0(R,\Phi) = \int_0^R h(r,\Phi) dr = 2aR - |\Phi| R^2/2. \tag{56}$$

Summing the diagrams Fig. 4(b) together with Fig. 4(a), one gets an exact equation

$$\frac{\delta\rho}{\rho} = \frac{nl_{\rm tr}}{4l}\mathrm{Re}\int_a^\infty \frac{dR}{R}e^{-2R/l}\int_0^{2\pi} d\varphi_0 \int_0^{2\pi} d\varphi_f\, \sigma(\varphi_0)\sigma(\varphi_f)$$

$$\times(1-e^{i\varphi_f})e^{nS_0(R,\Phi)} = \frac{2\beta_0}{3}\ln\left(\frac{C}{2\beta_0}\right), \qquad (57)$$

instead of the qualitative estimate Eq. (6).

Here $C\approx 1.8$ is a numerical coefficient. Thus, addition of the series Fig. 4(b) to Fig. 4(a) leads to the following renormalization: $\ln(1/2\beta_0)\to\ln(C/2\beta_0)$.

F. Estimate for neglected diagrams

In this section we use the derivation presented in the preceding section to show how to select relevant diagrams. The derivation was based on identity (52). The left-hand side of this equation is proportional to the impurity cross section $\sigma(\alpha-\alpha')\sim a$. However, the right-hand side is parameterically larger $\sim R$, provided that $|\alpha-\alpha[\mathbf{R}]|<a/R$. One can show that the function similar to the one on the right-hand side (52) arises each time when one of the index μ or ν in the pairing $\langle\delta T^\mu\delta T^\nu\rangle$ is equal to $(-)$. [for a pairing $\langle\delta T^-\delta T^-\rangle$ we have two functions of the type (52) see Eq. (53)]. For the case when μ or ν equals to $(+)$ we have a differential cross section $\sigma(\alpha-\alpha[\mathbf{R}])\sim a$ instead of function (52). Now we are ready to estimate different types of diagrams. Insertion of one additional $(-,-)$ pairing into a diagram in Figs. 5–8 gives two additional Green's functions and, consequently, multiplier $\sim 1/l^2$ and two functions of the type (52) giving a multiplier $\sim l^2$. One should also multiply on disk concentration n and integrate over $d\mathbf{R}$. Due to θ functions in Eq. (52) the integration area $d\mathbf{R}$ is of the order la. Combining all the multipliers together we have $nla\sim 1$. Therefore, addition of $(-,-)$ pairing does not lead to any smallness. In contrast to this, insertion of $(-,+)$ pairing leads to smallness $\sim a/l$. Indeed, the only difference from the case of $(-,-)$ pairing is that one should replace one of the functions (52) by the corresponding cross section. This leads to the change of one of the multiplier of the order l by multiplier of the order a. Following this line of reasoning one could conclude that insertion of $(+,+)$ pairing leads to the smallness of the order of $(a/l)^2$ Actually, the smallness arising from insertion of $(+,+)$ pairing is of the order of a/l. Indeed, while the replacement of each of the two functions of the type (52) the corresponding cross section leads to the relative smallness of the order $(a/l)^2$, the integration area in this case is not restricted by angle dependent θ functions. As a result, the integration area, $d\mathbf{R}\sim l^2$, is larger by a parameter l/a compared to the case of $(-,-)$ pairing. Note that estimates presented above do not work for the diagrams with one dashed line Figs. 5–8. In this case one should integrate over initial and final scattering angles. One can easily see that integration of Eq. (52) over angle α leads to the multiplier of the order of a. This implies that in this case all four pairings, $(++)$, $(+-)$, $(-+)$, and $(--)$ are of the same order, of a/l [see Eq. (41)]. Note that the higher order diagrams which are small in the parameter β_0 may turn out to be relevant for the MR at very low magnetic field (see Sec. IV).

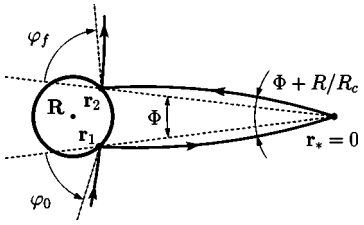

FIG. 13. The magnetic field changes the backscattering angle $\phi=\Phi+R/R_c$. The dashed (solid) line in represents electron trajectory for $B=0$ ($B\neq 0$). The electron trajectory for $B\neq 0$ is parametrized by the scattering angles $B=0$.

G. Anomalous magnetoresistance

In this section we generalize our calculations for the $B\neq 0$ case assuming that B is small ($\beta\ll 1$). The main contribution in this case still comes from diagrams in Figs. 4(a) and 4(b). Consider for example diagram $(++)$. Let us compare the process of double scattering described by this diagram for $B\neq 0$ (see Fig. 13) with the same process for $B=0$ (see Fig. 5). For fixed points $\mathbf{r}_1$, $\mathbf{r}_2$, and $\mathbf{r}_*=0$, one can see the following differences. First, the scattering angles φ_0 and φ_f acquire small corrections of the order of $R/R_c\sim l/R_c=\beta\ll 1$. Second, the parts of the electron trajectory corresponding to free ends of the picture become curved. The backscattering angle ϕ increases by the value R/R_c

$$\phi = \Phi + R/R_c, \qquad (58)$$

where Φ is the value of backscattering angle for $B=0$ given by Eq. (55). Finally, the overlap area of the corridors changes because the trajectories become curved (see Fig. 13). The corrections to φ_0 and φ_f lead to small relative corrections to the resistivity of the order of $\beta_0\beta^2$ and can be neglected. The same reason allows one to neglect the curvature of the incoming and outgoing parts of the trajectory. Therefore, the only relevant difference is the change of the overlap area of the corridors. The solution of the Dyson equation is analogous to the $B=0$ case. The points of intermediate integration $\mathbf{r}$ and $\mathbf{r}'$ lie now at the segments of cyclotron circles (from $\mathbf{r}_1$ to $\mathbf{r}_*$ and from $\mathbf{r}_*$ to $\mathbf{r}_2$). The pairing of two operators $\delta\hat{T}^-$ is still given by Eq. (47) with the replacement $h(r)\to h_B(r)$. For $\beta,\beta_0\ll 1$, the overlap width is calculated as

$$h_B(x)\approx(2a-|\phi r-r^2/R_c|)\,\theta(2a-|\phi r-r^2/R_c|), \qquad (59)$$

where θ is the Heaviside step function. Therefore, the only difference from Eq. (57) is that one should replace $S_0\to S_B$, where the overlap area is given by

$$S_B(R,\phi)=\int_0^R dr\, h_B(r), \qquad (60)$$

The value of $\delta\rho_{xx}/\rho$ is obtained from Eq. (57) by replacing e^{nS_0} to $e^{nS_B}-e^{nS_0}$,

$$\frac{\delta\rho_{xx}}{\rho}=\frac{nl_{\rm tr}}{4l}{\rm Re}\int_a^\infty\frac{dR}{R}e^{-2R/l}\int_0^{2\pi}d\varphi_0\int_0^{2\pi}d\varphi_f\,\sigma(\varphi_0)\sigma(\varphi_f)$$
$$\times(1-e^{i\varphi_0})(1-e^{i\varphi_f})(e^{nS_B(R,\Phi)}-e^{nS_0(R,\Phi)}). \qquad (61)$$

Introducing dimensionless variables $T=R/l$, $z=\beta/\beta_0$ we get Eq. (1), where function $f(z)$ is given by

$$f(z)=\frac{3}{32}\int_0^\infty\frac{dT}{T}e^{-2T}\int_0^{2\pi}d\varphi_0\int_0^{2\pi}d\varphi_f$$
$$\times\cos\left(\frac{\varphi_0+\varphi_f}{2}\right)\sin^2\left(\frac{\varphi_0}{2}\right)\sin^2\left(\frac{\varphi_f}{2}\right)(e^{s_z}-e^{s_0}). \qquad (62)$$

Here

$$s_z=\int_0^T dt\left(1-\left|\zeta t-\frac{zt^2}{2}\right|\right)\theta\left(1-\left|\zeta t-\frac{zt^2}{2}\right|\right),$$

$$\zeta=\frac{\cos(\varphi_0/2)+\cos(\varphi_f/2)}{2T}+\frac{zT}{2},\quad s_0=s_{z\to 0}. \qquad (63)$$

Function $f(z)$ has the following asymptotics:

$$f(z)=\begin{cases}0.32z^2 & \text{for } z\to 0,\\ 0.39-1.3/\sqrt{z} & \text{for } z\to\infty.\end{cases} \qquad (64)$$

In the interval $0.05\lesssim z\lesssim 2$, $f(z)$ can be well approximated by the linear function

$$f(z)\approx 0.032(z-0.04)\quad \text{for } 0.05\lesssim z\lesssim 2. \qquad (65)$$

Next we discuss the parabolic asymptotics more carefully. We will show that in this asymptotic region there are two contributions of different signs to the magnetoresistance: a negative contribution coming from the trajectories with very small Φ such that $|\Phi|\lesssim\beta$, and a positive contribution coming from larger angles. This considerations will be used in the next section, discussing trajectories with the long Lyapunov region.

First, we write the difference of two exponents $e^{nS_B}-e^{nS_0}$ as follows $(e^{n(S_B-S_0)}-1)e^{nS_0}$ and expand the equation in the bracket in the Taylor expansion up to the second order,

$$e^{nS_B}-e^{nS_0}\approx e^{nS_0}\left(n\delta S+\frac{n^2\delta S^2}{2}\right),$$

$$\delta S=S_B-S_0. \qquad (66)$$

We consider the case $z\ll 1$ $(\beta\ll\beta_0)$. One can easily see that in this case the expression $2a-|\phi r-r^2/R_c|$, entering in the argument of θ function in Eq. (59) is positive at all values of Φ [we take into account Eq. (55) and have in mind that $r\lesssim l$]. Therefore, the difference $\delta S(\Phi)=S_B(\Phi)-S_0(\Phi)$ is expressed as

$$\delta S(\Phi)=\int_0^R dr\,r(|\Phi|-|\Phi+(R-r)/R_c|)$$
$$=\begin{cases}-\dfrac{R^3}{6R_c} & \text{for } \Phi>0,\\ +\dfrac{R^3}{6R_c}-\dfrac{(R+R_c\Phi)^3}{3R_c}\theta(R+R_c\Phi) & \text{for } \Phi<0.\end{cases} \qquad (67)$$

To sum the contributions of different electron trajectories, we take into account that the time reversed trajectories have the same statistical weight. Indeed, as seen from Figs. 5–8 and 13, time reversion correspond to the change $\varphi_0\to 2\pi-\varphi_f$, $\varphi_f\to 2\pi-\varphi_0$. This transformation does not affect the factor $\sigma(\varphi_0)\sigma(\varphi_f)(1-e^{i\varphi_0})(1-e^{i\varphi_f})$, entering Eq. (61). At the same time, the angle Φ changes to $-\Phi$ under this transformation [see Eq. (55)]. From Eq. (67) we find the variation of the overlap area averaged over two time reversed trajectories,

$$n\frac{\delta S(\Phi)+\delta S(-\Phi)}{2}=-\frac{n(R-R_c|\Phi|)^3}{6R_c}\theta(R-R_c|\Phi|). \qquad (68)$$

This expression is of the order of β/β_0 for $|\Phi|<R/R_c\sim\beta$ and is equal to zero for larger angles. We conclude therefore, that time reversed contributions do not cancel only in the region of small angles $\Phi\lesssim\beta$. Since the total variation of Φ is much larger, of the order of β_0 [see Eq. (55)], we can replace the expression on the right-hand side of Eq. (68) by δ-function, writing $n(\delta S(\Phi)+\delta S(-\Phi))/2\approx-(\beta^2/24\beta_0)(R^4/l^4)\delta(\Phi)$. Keeping the leading terms of the order of β^2 only, we obtain

$$\frac{e^{n\delta S(\Phi)}+e^{n\delta S(-\Phi)}}{2}-1\approx-\frac{\beta^2}{24\beta_0}\frac{R^4}{l^4}\delta(\Phi)+\frac{\beta^2}{(24\beta_0)^2}\frac{R^6}{l^6}. \qquad (69)$$

The second term in this equation comes from the averaging of the quadratic term in the exponent expansion $n^2\delta S^2/2$ over two time reversed trajectories. This term is positive and partly compensates the negative contribution of small angles. Using Eqs. (55), (56), and (61), after some algebra we get the low-field asymptotic of MR as the sum of the negative and positive contributions discussed above

$$\frac{\delta\rho_{xx}}{\rho}=-\frac{\beta^2}{2\beta_0}+A\frac{\beta^2}{\beta_0}\approx-0.32\frac{\beta^2}{\beta_0}, \qquad (70)$$

where numerical coefficient A is given by

$$A=320\int_0^\pi\int_0^\pi d\alpha\,d\beta\frac{\sin^2\alpha\sin^2\beta\cos(\alpha+\beta)}{(4+\cos\alpha-\cos\beta)^6}\approx 0.18. \qquad (71)$$

IV. CONTRIBUTION OF TRAJECTORIES WITH LONG LYAPUNOV REGION TO MAGNETORESISTANCE

The equations derived in the preceding section give the contribution to the MR related to the processes shown in

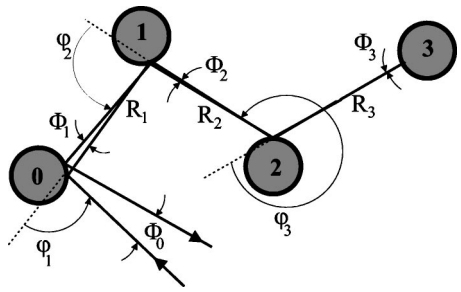

FIG. 14. Electron trajectory with a Lyapunov region, containing $N=3$ correlated links.

Figs. 5–8, the parabolic asymptotics (70) starting to work when β becomes smaller than β_0. Such processes are related to the correlations specific for returns to the initial point after one scattering. As we show at this section for very low magnetic fields, $\beta \ll \beta_0^2$, other correlations come into play. Specifically, we consider the contribution to the MR of the trajectories containing long Lyapunov regions. Such trajectories consist of the direct and the return paths and involve real double scatterings on some number of disks as shown in Fig. 14. The divergency between the direct and the return paths is characterized by the Lyapunov length. We will call such trajectories "Lyapunov trajectories." In the diagrammatic series they are presented by the sum of the diagrams shown in Fig. 15. Just as in the case discussed above, four different pairings are allowed at the ends of external dashed lines: $(-,-)$, $(+,-)$, $(-,+)$ and $(+,+)$. However, in contrast to the diagrams shown in Fig. 4, internal lines of "Lyapunov diagrams" contain pairings of $(+,+)$ type as well as of $(-,-)$ type. Physically, $(+,+)$ pairings corresponds to real double scatterings in the Lyapunov region. We will count such diagrams by the number N of correlated links in the Lyapunov region. The Lyapunov trajectory shown in Fig. 14 corresponds to $N=3$. The diagrams in Fig. 4 discussed in Sec. III, present a particular case of diagrams with Lyapunov region, corresponding to $N=1$. The correlated links of any Lyapunov trajectory are renormalized by the pairings $(-,-)$ as was discussed already for $N=1$. The contribution of any diagram of such type to the resistivity is small as β_0^N. However, as will be shown below, these diagrams have a sharp dependence on the magnetic field at very small fields. We will show that for $\beta < \beta_0^N$ the diagram of the Nth order gives a contribution to the parabolic MR of the same order as the contribution of the diagrams with $N=1$ already calculated above.

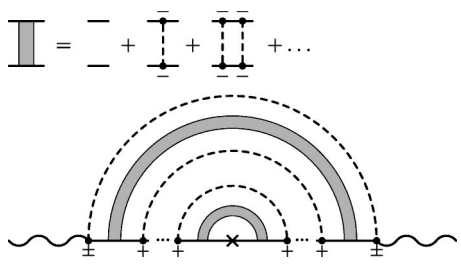

FIG. 15. The diagrams corresponding to electron trajectories with long Lyapunov regions.

Consider the Lyapunov trajectory with N correlated links. Denote by $\Phi_0, \Phi_1, \ldots, \Phi_N$ the angles between the segments of the direct and the return paths and by $\varphi_0, \ldots, \varphi_{N-1}$ the scattering angles between successive correlated links as shown in Fig. 14. The contribution of such a process has a sharp dependence on the magnetic field due to the magnetic field dependence of the overlap of the corridors surrounding the direct and the return path. This dependence is different for different segments of the trajectory due to the difference of the angles Φ_n. Indeed as we have seen in the preceding section if Φ is the typical angle between the direct and the return paths then the characteristic scale for the magnetic field dependence of the overlap of the corridors is $\beta \sim \Phi$. As one can see from Eq. (55), the typical value of the angle Φ_n is of the order β_0^n. The smallest angle $\Phi_N \sim \beta_0^N$ corresponds to the last segment of the trajectory. Therefore it is this segment that should lead to the sharpest dependence of the resistivity on the magnetic field. Consider the contribution of the last segment at small magnetic field $\beta \ll \beta_0^N$. For typical trajectories with $\Phi_N \sim \beta_0^N$ there is a cancellation of the contributions of the time reversed paths to the MR (see discussion in the preceding section). However, for a small fraction of the trajectories with $\Phi_N \lesssim \beta$ the contribution of the time reversed paths does not cancel and is proportional to the change of the overlap area $n(\delta S(\Phi_N) + \delta S(-\Phi_N))/2 \sim \beta/\beta_0$. The phase space of such trajectories is proportional to β/β_0^N. Thus, the contribution of the Lyapunov trajectory with N links to the resistivity in the region of small magnetic field is given by

$$\frac{\delta\rho_{xx}^N}{\rho} \sim -\beta_0^N \frac{\beta}{\beta_0}\frac{\beta}{\beta_0^N} \sim -\frac{\beta^2}{\beta_0} \quad \text{for } \beta < \beta_0^N, \tag{72}$$

where the factor β_0^N is due to the Nth order of the corresponding diagram. As we show below, the coefficient in this equation does not depend on the diagram order. It equals $1/2$, thus coinciding with the coefficient in the small angles contribution to parabolic asymptotic for $N=1$ [see Eq. (70)]. It is worth noting that only in the case $N=1$, one should take into account the contribution of large angles, presented by the second term in Eq. (70). For $N>1$ such contribution is parametrically small.

Before presenting rigorous derivation of above statements, we consider qualitatively the contribution of Nth order diagram for larger magnetic fields $\beta > \beta_0^N$. At such fields the first order contribution of the time reversed paths to the corridor effect does not cancel for trajectories with any values of Φ up to the maximal value $\Phi \sim \beta_0^N$. Thus, the factor β/β_0^N, which counts the phase space of relevant trajectories saturates at some constant value of the order of unity and one has

$$\frac{\delta\rho_{xx}^N}{\rho} \sim -\beta\beta_0^{N-1} \quad \text{for } \beta > \beta_0^N. \tag{73}$$

Consider now the MR in the interval $\beta_0^{N+1} < \beta < \beta_0^N$. In this interval the Lyapunov trajectories with the number of double scatterings smaller than N give a parabolic contribution Eq. (72) to the MR. The trajectories with the number of double scatterings bigger than n give a linear contribution Eq. (73), the main contribution $\beta_0^N\beta$ coming from the trajec-

tories with $N+1$ double scattering. As a result one has

$$\frac{\delta\rho_{xx}}{\rho} \approx -\left(\frac{N}{2}-A\right)\frac{\beta^2}{\beta_0} - C_N\beta_0^N\beta \quad \text{for } \beta_0^{N+1} < \beta < \beta_0^N. \tag{74}$$

Here $C_N \sim 1$ and A is given by Eq. (71). For $N \gg 1$ the second term on the right-hand side of Eq. (74) can be neglected and we get finally

$$\frac{\delta\rho_{xx}}{\rho} \approx -\frac{N}{2}\frac{\beta^2}{\beta_0} \quad \text{for } \beta_0^{N+1} < \beta < \beta_0^N,\ N \gg 1. \tag{75}$$

Equation (74) indicates that at very low magnetic fields, which correspond to large $N \sim \ln\beta/\ln\beta_0$ the results of Sec. III G. become incorrect and logarithmic renormalization of the parabolic MR occurs,

$$\frac{\delta\rho_{xx}}{\rho} \approx -\frac{\ln\beta}{2\ln\beta_0}\frac{\beta^2}{\beta_0}. \tag{76}$$

Next we present a rigorous derivation of the contribution of the Nth order Lyapunov trajectory for $\beta \ll \beta_0^N$. As follows from qualitative considerations presented above, $\Phi_n \ll 1$ for any $0 \leqslant n \leqslant N$. Indeed, $\Phi_n \sim \beta_0^n\Phi_0$. Since the minimal angle, Φ_N is on the order of β the maximal angle is small compared to unity, $\Phi_0 \sim \beta/\beta_0^N \ll 1$. Therefore, the direct and return paths of the relevant Lyapunov trajectories are very close to each other. This allows us to characterize a scattering between $n-1$ and n links of the trajectory by one scattering angle φ_n instead of two different scattering angles for direct and return paths. The dependence on the magnetic field comes from the last link of the trajectory. Expanding $e^{n(S_B^N-S_0^N)}-1$, like it was done in the preceding section, we only keep the first term,

$$n\frac{\delta S(\Phi_N)+\delta S(-\Phi_N)}{2} \approx -\frac{\beta^2}{24\beta_0}\frac{R_N^4}{l^4}\delta(\Phi_N). \tag{77}$$

To write down the analytical expression for Nth order contribution we should take into account for combinations of $(\pm,\pm)$ at the ends of the diagram in Fig. 15. This corresponds to four types of scattering on the impurity 0 in Fig. 14 and leads to appearance of the factor $(1-e^{i\varphi_1})(1-e^{i\varphi_1'}) = |1-e^{i\varphi_1}|^2$. Here we took into account that direct and return paths coincide in the first approximation and, as a consequence, scattering angles φ_1, φ_1' for direct and return paths are related to each other as follows: $\varphi_1 = 2\pi - \varphi_1'$. The analytical expression for MR is given by

$$\frac{\delta\rho_{xx}^N}{\rho} = -\frac{n^N l_{\mathrm{tr}}}{4l}\int d\varphi_1\, d\Phi_0\, d^2\mathbf{R}_1 \cdots d^2\mathbf{R}_N |1-e^{i\varphi_1}|^2 \times \frac{\sigma^2(\varphi_1)e^{-R_1/l}}{R_1^2}\cdots\frac{\sigma^2(\varphi_N)e^{-R_N/l}}{R_N^2}\frac{\beta^2}{24\beta_0}\frac{R_N^4}{l^4}\delta(\Phi_N). \tag{78}$$

Here we integrate over distances between disks instead of integration over disks positions. The factors $\sigma^2(\varphi_n)$ comes from double scatterings, the factor R_n^2 from denominators of the two Green's functions, describing the propagation along the nth link on the direct and return way. In writing Eq. (78) we also took into account the renormalization of correlated links by the $(-,-)$ pairings. As a consequence of this renormalization nth link, which is passed twice (on the direct and return paths) comes with the factor $e^{-R_n/l}$ instead of $e^{-2R_n/l}$. What remains to do is to express the final angle Φ_N via the initial angle Φ_0. From simple geometric considerations we get

$$\Phi_0 = \frac{R_1}{\sigma(\varphi_1)}\cdots\frac{R_N}{\sigma(\varphi_N)}\Phi_N. \tag{79}$$

Combining Eqs. (78) and (79) and performing the integral one gets

$$\frac{\delta\rho_{xx}^N}{\rho} = -\frac{1}{2}\frac{\beta^2}{\beta_0} \quad \text{for } N > 1. \tag{80}$$

V. INTERPRETATION OF THE RESISTIVITY CORRECTION IN TERMS OF SMALL CHANGE OF THE EFFECTIVE SCATTERING CROSS SECTION

In our calculations of resistivity corrections we used Eq. (8) as a starting point. Here we briefly discuss an alternative approach based on the accounting of the memory effects in terms of small change of the effective cross section. Consider first the $(+,+)$ ballistic returns with given values of the angles φ_0 and φ_f. The contribution of such processes to the resistivity (both for $B=0$ and for $B\neq 0$) contains the factor $\mathrm{Re}\, e^{i(\varphi_0+\varphi_f)} = \cos(\varphi_0+\varphi_f)$. Let us introduce now the scattering angle φ for the process $(+,+)$ considered as a single scattering on a complex scatterer. For small values of φ_0 and φ_f this angle is evidently given by $\varphi = \pi+\varphi_0+\varphi_f$. For arbitrary values of φ_0, φ_f the scattering angle reads

$$\varphi = \varphi_{\varphi_0,\varphi_f} = (\pi+\varphi_0+\varphi_f)(\mathrm{mod}\, 2\pi). \tag{81}$$

Such definition ensures that $0 < \varphi < 2\pi$. Next we introduce the integration over this angle: $\int d\varphi_0\, d\varphi_f \cos(\varphi_0+\varphi_f)\cdots = (-1)\int d\varphi \cos\varphi \int d\varphi_0\, d\varphi_f\, \delta(\varphi-\varphi_{\varphi_0,\varphi_f})\cdots$. Analogous expressions can be easily written for the processes $(-,-)$, $(+,-)$, and $(-,+)$. As a result, one can write the contribution of four possible types of correlations as follows:

$$\mathrm{Re}\int d\varphi_0\, d\varphi_f (1-e^{i\varphi_0})(1-e^{i\varphi_f})\cdots = -\int d\varphi\cos\varphi\int d\varphi_0\, d\varphi_f (\delta(\varphi-\varphi_{\varphi_0,\varphi_f}) + \delta(\varphi-\pi) - \delta(\varphi-\varphi_{\varphi_0,0}) - \delta(\varphi-\varphi_{0,\varphi_f}))\cdots . \tag{82}$$

The $(-,-)$ process is represented in Eq. (82) by $\delta(\varphi-\pi)$. Here we neglected a small difference (on the order of β_0) between the angle φ and π. By virtue of Eq. (82) one can easily check that the memory effects related to four types of ballistic returns can be accounted quantitatively in the frame of the usual Boltzmann equation. One should just replace the scattering cross-section on one disk $\sigma(\varphi)$ by the effective cross section

$$\sigma_{\rm eff}(\varphi) = \sigma(\varphi) + \delta\sigma_B(\varphi), \tag{83}$$

where $\delta\sigma_B(\varphi)$ is the field-dependent correction given by

$$\delta\sigma_B(\varphi) = \frac{1}{4l}\int_a^\infty \frac{dR}{R} e^{-2R/l} \int_0^{2\pi} d\varphi_0 \int_0^{2\pi} d\varphi_f \, \sigma(\varphi_0) \times \sigma(\varphi_f) e^{nS_B} [\delta(\varphi - \varphi_{\varphi_0,\varphi_f}) + \delta(\varphi - \pi) - \delta(\varphi - \varphi_{\varphi_0,0}) - \delta(\varphi - \varphi_{0,\varphi_f})]. \tag{84}$$

This correction does not change the total cross section

$$\int_0^{2\pi} d\varphi \; \delta\sigma_B(\varphi) = 0. \tag{85}$$

In other words, the enhancement of cross section caused by processes $(+,+)$ and $(-,-)$ is accompanied by the reduction of the scattering due to the $(+,-)$ and $(-,+)$ correlations. The resistivity correction is proportional to the change of the inverse transport length,

$$\delta\left(\frac{1}{l_{\rm tr}}\right) = n\int_0^{2\pi} d\varphi (1 - \cos\varphi)\, \delta\sigma_B(\varphi) = -n\int_0^{2\pi} d\varphi \cos\varphi \; \delta\sigma_B(\varphi). \tag{86}$$

Using Eqs. (82), (83), and (86) one can easily get Eq. (61) for MR.

Finally we note that this approach is easily generalized for calculation of the contribution of the trajectories having long Lyapunov region. For such trajectories one should replace the angles φ_0 and φ_f in Eq. (82) by φ_1 and $\varphi_1' \approx 2\pi - \varphi_1$ (see Sec. IV). For very small β such that $\beta_0^{N+1} < \beta < \beta_0^N$ and $N \gg 1$, the magnetic field induced correction to the scattering cross-section is expressed in a simple form,

$$\frac{\delta\sigma_B(\varphi) - \delta\sigma_0(\varphi)}{2a} \approx -\frac{2\beta^2 \ln\beta}{9\beta_0 \ln\beta_0}\left(\delta(\varphi - \pi) - \frac{\cos^2(\varphi/2)}{\pi}\right). \tag{87}$$

VI. DISCUSSION

In the preceding sections we derived analytical theory of the low-field anomaly in the magnetoresistance, caused by sharp dependence of the memory effects specific for backscattering events on the magnetic field. Next we compare our calculations with the results of simulations and with experiment. Note first that there is a parametrically small nonanomalous correction to Eq. (1) due to returns after multiple scatterings. This correction is given by[16]

$$\delta\rho_{xx}'/\rho \approx -0.2\beta_0\beta^2.$$

To compare the results of simulations[16] with the theoretical results in a wider region of parameters β, β_0, we substract $\delta\rho_{xx}'/\rho$ from the numerical curves. Theoretical and numerical[16] results are plotted in Fig. 16, in the universal units, $\delta\rho_{xx}/\rho\beta_0$ versus $z = \beta/\beta_0$. It is seen, that the theoretical and numerical results are in very good agreement. Experimental measurement of the MR in the system of antidot arrays[18] agrees qualitatively with our predictions. The experimentally observed MR was linear in magnetic field in a wide region of fields. This region corresponds to the interval of magnetic fields, where our results can be approximated by linear dependence [see Eq. (2)]. The magnetic fields used in experiment were relatively strong, and the parabolic asymptotic was not achieved. The quantitative comparison with the experiment[18] is more difficult due to several reasons. First of all, in the structures, used in experiment, besides antidots there were also short range scatterers. Our preliminary estimates show that accounting for a short range disorder can change the results of the calculations. Second, the antidot distribution was not fully chaotic in the experiment. To be more specific, the antidots were randomly moved from the regular square lattice distribution by shifts on the order of 30–40% of the lattice constant. Finally, the antidots did not have equal sizes, the uncertainty of the size being on the order of 50%. In spite of this, a very good quantitative agreement with the experiment can be achieved by appropriate choice of the antidot size a in the uncertainty interval (see also discussion of the experiment in Ref. 16). Note also that generalization of the theory for the case when antidot sizes vary is straightforward. What must to be done is to average pairings $\langle \delta\hat{T}^\mu \delta\hat{T}^\nu \rangle$ with the distribution function for the antidots sizes. This leads to the following modification of the obtained formulas: one should change $\sigma(\varphi_0)\sigma(\varphi_f) \to \overline{\sigma(\varphi_0)\sigma(\varphi_f)}$ in Eq. (57) and $h_B \to \overline{h_B}$ in Eq. (59). Here over line means averaging over antidot sizes. We do not present here corresponding calculations, since the distribution function of antidot sizes is not known for experiment.[18]

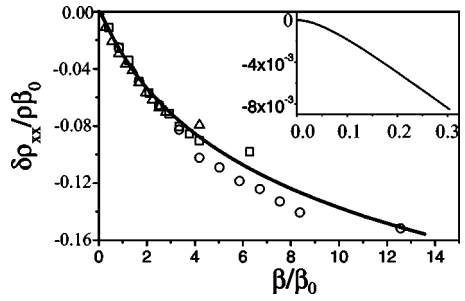

FIG. 16. The value of $\delta\rho_{xx}/\rho\beta_0$ from Eqs. (1) and (62) (solid line) shown as a function of β/β_0 together with the results of numerical simulations (Ref. 16) presented for different values of β_0 (triangles for $\beta_0 = 0.09$, boxes for $\beta_0 = 0.06$, circles for $\beta_0 = 0.03$). Data for all numerical curves are shown for $\beta < 0.3$. Inset, the crossover from quadratic to a linear dependence at $\beta/\beta_0 \sim 0.05$. This crossover was not resolved in numerical simulations.

Next we briefly discuss several interesting unsolved problems. Note first that above consideration of Lyapunov trajectories is valid, provided that $N < 1/\beta_0$. Indeed, while calculating the Nth order diagrams we neglected small contributions of $(+,-)$ and $(-,+)$ pairings on the all correlated links. Accounting of such pairings is rather tricky and is out of scope of this paper. We expect, however, that such correlations may lead to a factor on the order of $(1 - c\beta_0)^N$ $(c \sim 1)$ in Eq. (79). Therefore, for $N > 1/\beta_0$ the contribution

of Lyapunov diagrams might become N dependent. This gives a low-field limit for our theory

$$\beta > \beta_0^{1/\beta_0}. \tag{88}$$

We conclude that the behavior of the MR in the limit $\beta \to 0$ remains so far unclear.

In our calculations we fully neglected quantum effects. Such effects should decrease the "effect of empty corridor" due to the diffraction on the edges of the disks. In the situations where the magnetic field is not very small, $\beta > \beta_0^2$, the neglecting of the diffraction effects is justified if $a \gg \sqrt{\lambda_F l}$ (λ_F is a Fermi wavelength). This criterion ensures that diffraction effects on the edges of the disks are not relevant at the scales of the order of l. In the opposite case, $a \ll \sqrt{\lambda_F l}$, the diffraction should destroy the "corridor effect," thus suppressing the anomalous MR. For small magnetic fields, when $\beta \ll \beta_0^2$, the criterion for negligibility of the diffraction becomes stronger, $a \gg \sqrt{\lambda_F L}$, where $L \sim l \ln(1/\beta)/\ln(1/\beta_0)$ is the characteristic size of the Lyapunov region. Another quantum effect which can be especially important from the point of view of the possible experimental realizations is the weak localization phenomena. The weak localization correction to the conductivity also has an anomalous dependence on the magnetic field. Moreover, the interpretation of the memory effects in terms of small change of effective cross section discussed in Sec. V is very close to the interpretation of weak localization phenomenon developed in Ref. 26. Similar to discussion in Sec. V, the coherent enhancement of backscattering amplitude caused by weak localization, is accompanied by reduction of coherent scattering in other directions, the total cross section does not change. The competition of the non-Markovian and the weak localization effects might result in new interesting phenomena. The study of such competition in a system with spin-orbit interaction can be especially interesting, because, in contrast to the weak localization correction, the "corridor effect" is not very sensitive to spin-orbit coupling. The detailed analysis of the quantum effects is a challenging problem which will be addressed elsewhere.

We did not investigate the temperature dependence of the phenomenon. This dependence is related to the scattering by phonons (or electron-electron scattering) neglected in our calculations. It worth noting that importance of the electron-phonon scattering is expected to increase with decreasing magnetic field. Indeed, the potential of the electron-phonon interaction depends on time, therefore restricting the maximal length of a trajectory with the Lyapunov region $L < L_{ph}$, where $L_{ph} \sim v_F \tau_{ph}$ and τ_{ph} is the temperature dependent characteristic time of the electron-phonon scattering. This implies that at small magnetic fields one should replace the logarithmic factor $\ln(\beta)/\ln(\beta_0)$, entering Eq. (76) by a temperature dependent coefficient of the order of L_{ph}/l.

VII. SUMMARY

We propose a theory of the negative anomalous MR in a system with strong scatterers. It is shown that the anomaly in the MR arises due to suppression of "empty corridor effect" by magnetic field. A detailed description of different types of non-Markovian correlations related to ballistic returns is presented. A method of diagrammatic expansion of the Liouville equation is developed which allows us to describe analytically the effects of "empty corridor" on ballistic returns. The analytical expressions for anomalous MR in different intervals of magnetic fields are derived [see Eqs. (1), (62), (64), and (74)]. The MR at very low magnetic fields was shown to be determined by the contribution of electron trajectories having long Lyapunov region. An interpretation of the memory effects in terms of small change of the effective scattering cross section is discussed. The analytical results are shown to be in very good agreement with the numerical simulations and experiment.

ACKNOWLEDGMENTS

The authors thank M. I. Dyakonov for insightful discussions and R. Jullien for providing us with the numerical data. We are also grateful to I. V. Gornyi and D. G. Polyakov for useful comments. The work was partially supported by RFBR, grant of Russian Scientific School, and by programmes of the RAS.

APPENDIX A

This Appendix contains the explicit expressions for the pairings $\langle \delta T^\mu \delta T^\nu \rangle$. Using Eqs. (13), (18), and (24), kernels of operators $\delta\hat{T}^+$, $\delta\hat{T}^-$, entering in Eq. (32) can be written as

$$\delta T^+_{\alpha,\alpha'} = \sigma(\alpha - \alpha')(n^+ - n),$$

$$\delta T^-_{\alpha,\alpha'} = -\delta(\alpha - \alpha')\delta T^-_\alpha, \tag{A1}$$

where

$$\delta T^-_\alpha = \int d\alpha''\, \sigma(\alpha - \alpha'')(n^- - n). \tag{A2}$$

The functions n^+ and n^- in Eq. (A1) depend on vectors $\mathbf{a}(\mathbf{n}', \mathbf{n})$ and $\mathbf{a}(\mathbf{n}'', \mathbf{n})$ correspondingly [see Eqs. (14) and (16)]. The pairings of operators $\delta\hat{T}^\mu$ and $\delta\hat{T}^\nu$ can be calculated with the use of Eqs. (30), (A1), and (A2). As a result we have

$$\langle \delta T^+_{\beta,\alpha_2}(\mathbf{r}_2)\delta T^+_{\alpha_1,\beta_0}(\mathbf{r}_1)\rangle = \sigma(\beta - \alpha_2)\sigma(\alpha_1 - \beta_0)J(-\mathbf{a}_{\beta,\alpha_2}, -\mathbf{a}_{\alpha_1,\beta_0}), \tag{A3}$$

$$\langle \delta T^-_\beta(\mathbf{r}_2)\delta T^-_{\beta_0}(\mathbf{r}_1)\rangle = \int d\alpha'\, d\alpha''\, \sigma(\beta - \alpha')\sigma(\beta_0 - \alpha'')J(\mathbf{a}_{\beta,\alpha'}, \mathbf{a}_{\beta_0,\alpha''}), \tag{A4}$$

$$\langle \delta T^+_{\beta,\alpha_2}(\mathbf{r}_2)\delta T^-_{\beta_0}(\mathbf{r}_1)\rangle = \sigma(\beta - \alpha_2)\int d\alpha'\, \sigma(\beta_0 - \alpha')J(-\mathbf{a}_{\beta,\alpha_2}, \mathbf{a}_{\beta_0,\alpha'}), \tag{A5}$$

$$\langle \delta T^{-}_{\beta}(\mathbf{r}_2)\delta T^{+}_{\alpha_1,\beta_0}(\mathbf{r}_1)\rangle = \sigma(\alpha_1-\beta_0)\int d\alpha'\ \sigma(\beta-\alpha') \times J(\mathbf{a}_{\beta,\alpha'},-\mathbf{a}_{\alpha_1,\beta_0}). \quad \text{(A6)}$$

Here function J emerges as a result of pairings of $\langle (n^{\mu}-n)\times(n^{\nu}-n)\rangle$ [see Eq. (30)] and is given by

$$J(\mathbf{a},\mathbf{b}) = n\int d\mathbf{R}\ \delta(\mathbf{r}_2-\mathbf{R}-\mathbf{a})\delta(\mathbf{r}_1-\mathbf{R}-\mathbf{b}). \quad \text{(A7)}$$

APPENDIX B

To calculate $\langle \delta T^{-}_{\alpha[\mathbf{r}_2]}(\mathbf{r})\delta T^{-}_{\alpha[-\mathbf{r}_1]}(\mathbf{r}')\rangle$ we first do the integral on the right-hand side of Eq. (A2). Integral of the term containing average density n is trivial and reduces to $1/l$. In the integral containing n^{-} it is convenient to introduce orthogonal coordinates x and y such that x axis is collinear with the velocity of the incident particle and write the delta function entering the definition (14) of n^{-} as $\delta(\mathbf{r}-\mathbf{R}_i-\mathbf{a}) = \delta(y-R_i^y-a_y)\delta(x-R_i^x-a_x)$. We proceed by lifting the y dependent delta function by integration over the angle α'. It is clear that the integral is vanishing for $|y-R_i^y|>a$. To calculate the integral for smaller $|y-R_i^y|$ note that by virtue of Eq. (16) $|da_y/d\alpha'| = |d(\mathbf{a}\times\mathbf{n})/d\alpha'| = \sigma(\alpha-\alpha')$ and therefore the integral of the y dependent delta function cancels the scattering cross section in Eq. (A2). As a result we get

$$\delta T^{-}_{\alpha}(\mathbf{r}) = 1/l - \sum_i \delta(x-R_i^x-a_x)\theta_i \approx 1/l - \sum_i \delta(x-R_i^x)\theta_i. \quad \text{(B1)}$$

Here θ_i is a unit step function which is equal to unity when $|y-R_i^y|<a$ and vanishes otherwise. Using Eq. (B1) we can write for backscattering angles close to π ($\Phi\sim a/l$),

$$\langle \delta T^{-}_{\alpha[\mathbf{r}_2]}(\mathbf{r})\delta T^{-}_{\alpha[-\mathbf{r}_1]}(\mathbf{r}')\rangle \approx nh(x,\Phi)\delta(x-x') \approx nh(r,\Phi)\delta(r-r'), \quad \text{(B2)}$$

where

$$h(r,\Phi) = (2a-|\Phi|r)\theta(2a-|\Phi|r)$$

is shown in Fig. 12.

[1] B. L. Altshuler, D. Khmelnitskii, A. I. Larkin, and P. A. Lee, Phys. Rev. B **22**, 5142 (1980).
[2] P. A. Lee and T. V. Ramakrishnan, Rev. Mod. Phys. **57**, 287 (1985).
[3] E. M. Baskin, L. N. Magarill, and M. V. Entin, Sov. Phys. JETP **48**, 365 (1978).
[4] A. V. Bobylev, F. A. Maaø, A. Hansen, and E.H. Hauge, Phys. Rev. Lett. **75**, 197 (1995).
[5] A. V. Bobylev, F. A. Maaø, A. Hansen, and E. H. Hauge, J. Stat. Phys. **87**, 1205 (1997).
[6] E. M. Baskin and M. V. Entin, Physica B **249**, 805 (1998).
[7] A. Kuzmany and H. Spohn, Phys. Rev. E **57**, 5544 (1998).
[8] D. Polyakov, Sov. Phys. JETP **63**, 317 (1986).
[9] M. Fogler, A. Dobin, V. Perel, and B. Shklovskii, Phys. Rev. B **56**, 6823 (1997).
[10] M. M. Fogler and B. I. Shklovskii, Phys. Rev. Lett. **80**, 4749 (1998).
[11] A. D. Mirlin, J. Wilke, F. Evers, D. G. Polyakov, and P. Wolfle, Phys. Rev. Lett. **83**, 2801 (1999).
[12] A. D. Mirlin, D. G. Polyakov, F. Evers, and P. Wolfle, Phys. Rev. Lett. **87**, 126805 (2001).
[13] D. G. Polyakov, F. Evers, A. D. Mirlin, and P. Wolfle, Phys. Rev. B **64**, 205306 (2001).
[14] D. G. Polyakov, F. Evers, and I. V. Gornyi, Phys. Rev. B **65**, 125326 (2002).
[15] A. Dmitriev, M. Dyakonov, and R. Jullien, Phys. Rev. B **64**, 233321 (2001).
[16] A. Dmitriev, M. Dyakonov, and R. Jullien, Phys. Rev. Lett. **89**, 266804 (2002).
[17] V. Cheianov, A. P. Dmitriev, and V. Yu. Kachorovskii, Phys. Rev. B **68**, 201304 (2003).
[18] G. Gusev, P. Basmaji, Z. Kvon, L. Litvin, Yu. Nastaushev, and A. Toporov, Surf. Sci. **305**, 443 (1994).
[19] J. Dorfman and E. Cohen, Phys. Lett. **16**, 124 (1965).
[20] J. Van Leeuwen and A. Weiland, Physica (Amsterdam) **36**, 457 (1967).
[21] J. Van Leeuwen and A. Weiland, Physica (Amsterdam) **38**, 35 (1968).
[22] E. H. Hauge, in *Transport Phenomena*, edited by G. Kirczenow and J. Marro, Lecture Notes in Physics, No. 31 (Springer, New York, 1974), p. 337.
[23] R. Peierls, *Surprises in Theoretical Physics* (Princeton University, Princeton, NJ, 1979).
[24] For $\beta\ll 1$ one can neglect the off-diagonal part of the conductivity tensor.
[25] R. Zwanzig, Phys. Rev. B **129**, 486 (1963).
[26] A. P. Dmitriev, I. V. Gornyi, and V. Yu. Kachorovskii, Phys. Rev. B **56**, 9910 (1997).